5-2018

On Permeability Prediction From Complex Conductivity Measurements Using Polarization Magnitude and Relaxation Time

Judith Robinson
Pacific Northwest National Laboratory

Lee Slater
Rutgers University-Newark

Andreas Weller
Technische Universität Clausthal

Kristina Keating
Rutgers University-Newark

Tonian Robinson
Rutgers University-Newark, tonianr@mail.usf.edu

See next page for additional authors

AGU100 ADVANCING EARTH AND SPACE SCIENCE

Water Resources Research

RESEARCH ARTICLE
10.1002/2017WR022034

Key Points:
- Sandstone permeability is well-predicted using complex conductivity models except where a high pore volume normalized surface area exists
- Geophysical length scales used in existing complex conductivity permeability models do not adequately account for variations in minerology
- Reliable in situ estimates of the electrical formation factor are a critical obstacle to field-scale implementation of permeability models

Supporting Information:
- Supporting Information S1
- Figure S1
- Figure S2
- Figure S3
- Figure S4

Correspondence to:
J. Robinson,
judith.robinson@pnnl.gov

Citation:
Robinson, J., Slater, L., Weller, A., Keating, K., Robinson, T., Rose, C., et al. (2018). On permeability prediction from complex conductivity measurements using polarization magnitude and relaxation time. *Water Resources Research*, *54*, 3436–3452. https://doi.org/10.1002/2017WR022034

Received 9 OCT 2017
Accepted 12 MAR 2018
Accepted article online 24 MAR 2018
Published online 16 MAY 2018

On Permeability Prediction From Complex Conductivity Measurements Using Polarization Magnitude and Relaxation Time

Judith Robinson[1], Lee Slater[2], Andreas Weller[3], Kristina Keating[2], Tonian Robinson[2], Carla Rose[4], and Beth Parker[4]

[1]Pacific Northwest National Laboratory, Richland, WA, USA, [2]Department of Earth and Environmental Sciences, Rutgers University-Newark, Newark, NJ, USA, [3]Institut für Geophysik, Technische Universität Clausthal, Clausthal-Zellerfeld, Germany, [4]G360 Institute for Groundwater Research, College of Engineering and Physical Sciences, University of Guelph, ON, Canada

Abstract Geophysical length scales determined from complex conductivity (CC) measurements can be used to estimate permeability k when the electrical formation factor F is known. Two geophysical length scales have been proposed: (1) the specific polarizability c_p normalized by the imaginary conductivity σ'' and (2) the time constant τ multiplied by a diffusion coefficient D_+. The parameters c_p and D_+ account for the control of fluid chemistry and/or varying minerology on the geophysical length scale. We evaluated the predictive capability of two CC permeability models: (1) an empirical formulation based on σ'' or normalized chargeability m_n and (2) a mechanistic formulation based on τ. The performance of the CC models was evaluated against measured k; and further compared against that of well-established k estimation equations that use geometric length scales. Both CC models predict permeability within one order of magnitude for a database of 58 sandstone samples, with the exception of samples characterized by high pore volume normalized surface area S_{por}. Variations in c_p and D_+ likely contribute to the poor model performance for the high S_{por} samples, which contain significant dolomite. Two observations favor the implementation of the σ''-based model over the τ-based model for field-scale k estimation: (1) a limited range of variation in c_p relative to D_+ and (2) σ'' field measurements are less time consuming to acquire relative to τ. The need for a reliable field-estimate of F limits application of either model, in particular the σ'' model due to a high power law exponent associated with F.

1. Introduction

The reliable in situ estimation of permeability remains one of the most challenging problems in hydrogeological characterization. Permeability can vary by orders of magnitude over short distances due to heterogeneity across multiple scales. Permeability is essential in the planning and implementation of water management projects including determining well yields, understanding recharge rates, and fluxes to surface water and designing storm water infrastructure. At environmental sites, permeability exerts a fundamental control on contaminant transport and determines the effectiveness of remediation strategies. Borehole tests to estimate permeability often do not fully capture site heterogeneity and may require upscaling to representative scales that determine flow and transport processes. Consequently, novel methods for measuring spatial variations of permeability at the field-scale are needed.

Indirect estimation of permeability is built upon equations that utilize a representative length scale associated with a dominant pore-scale dimension controlling fluid flow (Carman, 1939) coupled with an electrical formation factor F describing the ratio between tortuosity and porosity (Banavar & Johnson, 1987; Katz & Thompson, 1987, 1986). The models utilizing geometric length scales are summarized in Figure 1. Pape et al. (1987) proposed one such equation that is referred to as the PaRiS model. This model uses the inverse of the pore volume normalized surface area S_{por} as the representative length scale, with fitting parameters calibrated against a database composed of a wide range of sandstone samples. Another equation proposed by Banavar and Johnson (1987) is based on the Katz and Thompson (KT) model (Katz & Thompson, 1987). A dynamically interconnected pore radius Λ is derived from the mercury injection capillary pressure (MICP) method and used as the representative length scale in permeability estimation. In both cases, such

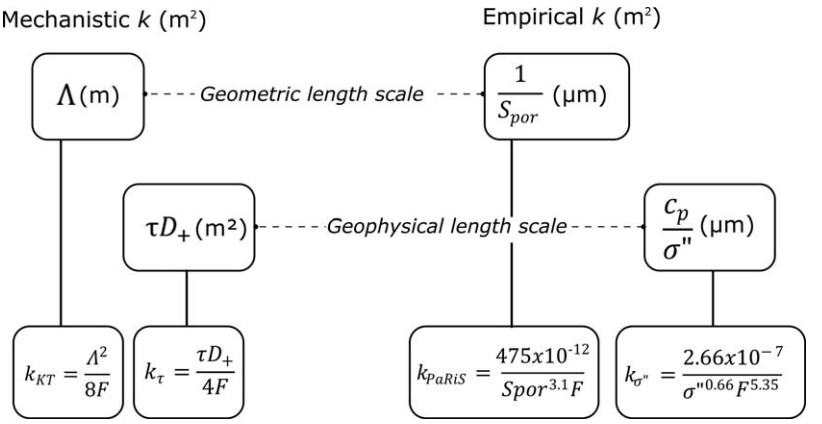

Figure 1. Graphical overview of geometric and geophysical length scales in relation to mechanistic (Banavar & Johnson, 1987; Katz & Thompson, 1987; Revil et al., 2015) and empirical permeability models (Pape et al., 1987; Weller et al., 2015a). Mechanistic length scales have units of L or L^2 (i.e., m or m^2). Empirical length scales have units of μm. The polarization magnitude model $k_{\sigma''}$ implicitly incorporates a single value of the specific polarizability, c_p

representative geometric length scales cannot be directly measured in situ, thereby limiting the application of these permeability prediction models at the field scale.

Geophysical measurements offer the possibility of indirectly determining representative length scales needed for in situ permeability prediction (Revil et al., 2012; Revil & Florsch, 2010; Slater, 2007). Using sensors placed on the surface and/or in boreholes, the variation of hydrogeological properties across multiple scales can be inferred from geophysical measurements (see Binley et al., 2015, for review). Complex conductivity (CC), often referred to as spectral-induced polarization (SIP), is an electrical geophysical method that provides measures that have been shown to be well correlated with representative geometric length scales controlling permeability (Binley et al., 2005; Scott & Barker, 2003; Slater, 2007). The low frequency ($<$1 kHz) CC response is determined by diffusive polarization mechanisms associated with ions in the electrical double layer (EDL) forming at the mineral-fluid interface. Both the magnitude and the relaxation time of this double layer polarization have been correlated with geometric length scales extracted from the grain or pore size distribution of the rock (Binley et al., 2005; Borner et al., 1996; Revil, 2013; Slater & Lesmes, 2002; Weller et al., 2010). Mechanistic and empirical models have been developed to explain the dependence of the CC parameters on geometric length scales derived from the pore or grain size distribution (Leroy et al., 2017, 2008; Revil et al., 2012; Weller et al., 2015a).

The link between CC parameters and representative geometric length scales has encouraged efforts to develop permeability prediction equations based on CC measurements as summarized in Figure 1. These models rely on a measure of the polarization strength (an imaginary conductivity σ'' or normalized chargeability term m_n) or the dominant relaxation time (typically a characteristic time constant τ) (Revil et al., 2015; Weller et al., 2015a). Unlike the geometric length scales $1/S_{por}$ and Λ, σ'' and τ are dependent on the pore filling fluid chemistry (Niu et al., 2016; Revil & Skold, 2011; Weller & Slater, 2012), surface mineralogy (Abuseda et al., 2016; Kruschwitz et al., 2016; Revil, 2012) and are a function of measurement frequency. Weller et al. (2011) introduced the concept of specific polarizability c_p, to represent the control of the fluid chemistry and/or mineralogy on polarization magnitude. Similarly, Revil (2013) defined values of a diffusion coefficient D_+ to accommodate such factors in a mechanistic model describing the CC of soils and rocks (Revil et al., 2015).

Accounting for the fluid conductivity and/or mineralogy controls on CC measurements allows equivalent geophysical length scales to be defined to replace the classical length scale appearing in the geometric models. These representative geometric length scales are defined as c_p/σ'' and τD_+ (Figure 1). They are coupled in permeability prediction equations with F, which is used to describe the porosity and tortuosity in the same way as the geometric models described above.

One such approach based on an electrical analog of the PaRiS model involves using a form of σ'' for S_{por}, as justified by the strong correlation between σ'' and S_{por} observed in numerous studies (e.g., Kruschwitz et al.,

2016; Weller et al., 2010). Similarly, an electrical analog of the Katz and Thompson (KT) model has been proposed where τD_+ is used as a proxy for Λ, a substitution that is justified by the strong empirical correlation between τ and pore radius observed in numerous studies (e.g., Revil et al., 2014). One challenge in using the equivalent geophysical length scales is uncertainty in the variation in c_p and D_+ associated with fluid chemistry and mineralogy. Using single values of c_p and D_+ to represent variations in the interfacial chemistry and mineralogy will limit the predictive capability of these permeability equations in natural settings where fluid chemistry and mineralogy vary (Kemna et al., 2012; Kruschwitz et al., 2010; Revil et al., 2012).

An inherent limitation of both the geometric (PaRiS, KT) and CC-based permeability predictions is that F must be known. Researchers have used MICP to estimate F (Amirtharaj et al., 2011; Katz & Thompson, 1987, 1986) with limited results due in part to unknown sample inhomogeneity (Amirtharaj et al., 2011). Reliable field-scale estimates of F are difficult (or impossible) to acquire unless pore fluid conductivity is very high (e.g., brine fluids) such that the surface conductivity is assumed negligible. Borner et al. (1996) first suggested that CC measurements could be used to estimate surface conductivity from σ'' measurements, allowing the measured real part of the conductivity to be corrected for surface conduction permitting a field-scale estimation of F. Several researchers have subsequently examined the relationship between σ'' and the surface conductivity measured using laborious multisalinity measurements both for sandstone (Revil et al., 2015; Weller et al., 2013) and limestone (Halisch et al., 2014) rocks in an attempt to generalize models for F estimation.

In this paper, we present a study using 58 sandstone samples where extensive physical and geophysical laboratory data were acquired. We examine the predictive capability of two recently proposed models of permeability estimation and use these models "as-is" with the predetermined constants and coefficients defined in the original models. Within the context of these two models, we: (1) explore the relative importance of the length scales (geometric and geophysical) and F on permeability prediction; (2) consider the limitations of CC permeability prediction due to the uncertainty in the parameters c_p and D_+ required to define geophysical length scales; and (3) investigate the effectiveness of proposed methods to estimate F by correcting for surface conductivity at low salinities using σ'' such that these permeability models could be applied to field scale CC data.

2. Permeability Models

2.1. PaRiS and Katz-Thompson (KT) Geometric Models

The PaRiS model is based on flow of fluid through a network of capillary tubes whereas the KT model is based on the application of percolation theory applied to a broad distribution of pore sizes. Central to both models is the definition of an effective hydraulic radius r_{eff} (μm) representative of the pore size controlling fluid flow. In the PaRiS equation, r_{eff} is related to S_{por},

$$r_{eff} \approx \frac{2}{S_{por}}, \tag{1}$$

$$S_{por} = S_s \rho_s \frac{1-\phi}{\phi}, \tag{2}$$

where S_s (m^2/g) is the specific surface area from Brunauer-Emmett-Teller (BET) analysis, ϕ is the porosity, and ρ_s is the density of the solids. In the KT equation, r_{eff} is equivalent to Λ (Banavar & Johnson 1987; Katz & Thompson 1986) as determined from MICP,

$$r_{eff} \approx \Lambda. \tag{3}$$

The PaRiS model is based on a modified Kozeny-Carman equation (Carman, 1939), where F replaces the ratio of the pore capillary tortuosity to the porosity (e.g., Guéguen & Palciauskas, 1994, p. 196). The PaRiS model also considers the fractal nature of internal surface roughness of sedimentary rocks. Pape et al. (1987) proposed the following model:

$$k_{PaRiS} = \frac{475}{Spor^{3.1} F} \tag{4}$$

where k_{PaRiS} is permeability predicted by the PaRiS model with originally presented units of Darcy (D) ($1\ D = 9.869 \times 10^{-13}\ m^2$) and where S_{por} is in μm^{-1}.

The KT permeability equation (Katz & Thompson 1986) is expressed as

$$k_{KT} = \frac{{l_c}^2}{cF}, \tag{5}$$

where k_{KT} (m^2) is permeability predicted by the KT model and l_c (μm) is the equivalent pore diameter corresponding to the pressure at which the maximum incremental mercury intrusion occurs using MICP. The constant c is a scaling constant equal to 226. Katz and Thompson (1986) equated l_c to the inflection point on the MICP cumulative pore size distribution curve, considered to represent the threshold at which the pore space of a rock becomes hydraulically interconnected (i.e., sufficient fluid saturation for fluid flow). Johnson et al. (1986) reformulated this original model in terms of Λ (μm) and Banavar and Johnson (1987) equating a pore radius ($l_c/2$) to Λ by a scaling constant a. This reformulation results in

$$k_{KT} = \frac{\Lambda^2}{8F}. \tag{6}$$

Modeling the pore network as a distribution of cylindrical pores of differing radii, Banavar and Johnson (1987) derived two scaling constants a (equal to 0.51 and 0.34) to represent different sizes of pores and multiplied $l_c/2$ by a to calculate Λ (i.e., $\Lambda = al_c/2$). Revil et al. (2014) equated equations (5) and (6) with $c=226$ (equation (5)) to derive a equal to 0.19.

2.2. Equivalent Geophysical Length Scale Models

Weller et al. (2015a) present an empirical model for permeability estimation that uses the inverse of the imaginary conductivity σ'' as the representative length scale. This is justified by the linear proportionality between σ'' and S_{por} demonstrated by Borner et al. (1996) and Weller et al. (2015b, 2010) where the linear coefficient represents the specific polarizability c_p (i.e., $\sigma'' = c_p S_{por}$) (in Siemens, S). Based on 58 clean and shaly sandstones samples from 17 formations, Weller et al. (2015a) presented a new empirical equation linking σ'' and F to permeability

$$k_{\sigma''} = \frac{2.66x10^{-7}}{{\sigma''}^{0.66} F^{5.35}}, \tag{7}$$

where $k_{\sigma''}$ (m^2) is the permeability predicted using σ'' (mS/m) at a frequency of 1 Hz. Weller et al. (2015a) implicitly incorporated a single value of c_p in equation (7), represented in the numerator. The value of c_p was previously found to be equal to 10×10^{-12} S for 114 samples (Weller et al., 2010), and 30×10^{-12} and 3×10^{-12} S for sandstones from the Bahariya Formation with a high and low magnetic susceptibility (greater than and less than 100×10^{-6} (dimensionless, SI units)), respectively (Abuseda et al., 2016). Using the methylene blue (MB) method to determine S_{por}, Weller et al. (2015b) found c_p equal to 7.5×10^{-12} S for 60 unconsolidated samples saturated with a conductive fluid with a conductivity close to 100 mS/m. Regardless of the sample or method used to determine S_{por}, values of c_p vary by at most one order of magnitude.

Rather than relying on a single frequency measure of σ'', a Debye decomposition approach can be used to integrate over a range of frequencies to give a measure of the polarization strength that encompasses the frequency dependence of the CC response (Nordsiek & Weller, 2008). Weller et al. (2015a) also considered the normalized chargeability m_n obtained from a Debye decomposition where the equivalent predictive equation is

$$k_{m_n} = \frac{8.69x10^{-7}}{m_n^{0.79} F^{5.38}}, \tag{8}$$

where k_{m_n} (m^2) is the permeability predicted using m_n (mS/m). Again, the numerator value of 8.69×10^{-7} implicitly incorporates a single value of c_p. Equations (7) and (8) will be referred to herein as geophysical polarization magnitude permeability models.

Revil et al. (2012) present a mechanistic model based on the KT model (equation (6)) for permeability estimation using the CC relaxation time τ (s) (the exact definition of this parameter is discussed below) in conjunction with a diffusion coefficient D_+ (m^2/s) as a representative length scale. This development is built on

work originally based on spherical particles in suspension (Schwarz, 1962), where the relaxation time τ is related to the grain size radius, R by,

$$\tau = \frac{R^2}{2D_+}, \tag{9}$$

with D_+ related to the effective ionic mobility β^s_+, temperature T, the Boltzmann's constant k_b, and the charge of counterions in the Stern layer q_+ by the Nernst-Einstein relationship $D_+ = k_b T \beta^s_+ / |q_+|$. Based on different β^s_+ values for a shaly-sand (Vinegar & Waxman, 1984) and unconsolidated sand sediments (Koch et al., 2011), Revil (2013) and Revil et al. (2012) proposed two values of D_+: 1.3×10^{-9} m^2/s for clean sands and 3.8×10^{-12} m^2/s for clayey material. Revil et al. (2012) proposed that τ is related to Λ by

$$\tau = \frac{\Lambda^2}{2D_+}. \tag{10}$$

Substitution of equation (10) into equation (6) yields the permeability prediction model proposed by Revil et al. (2012)

$$k_\tau = \frac{\tau D_+}{4F}. \tag{11}$$

The application of equation (11) for permeability prediction is reliant on an accurate estimate of D_+. The k_τ model will be referred to herein as the geophysical time constant permeability model.

3. Sample Descriptions and Methods

Our sample database consists of 58 sandstone samples where hydraulic and physical property measurements (permeability, BET specific surface area, MICP pore size distribution, porosity) as well as CC spectral data and/or parameters are recorded.

3.1. Santa Susana and Hydrite Samples

The majority of our database is composed of 43 previously unpublished samples from two sites: the Santa Susana Field Laboratory (California, USA) with 22 samples and the Hydrite Chemical Company (Wisconsin, USA) with 21 samples. The Santa Susana site is a Cretaceous age deep-sea turbidite deposit composed primarily of sandstone with minor interbeds of shale and siltstone and occasional conglomerate of similar mineralogy. The sedimentary rocks at the Hydrite site are Cambrian to Ordovician in age and are associated with a variety of marine, shoreface, and terrestrial depositional environments. Consequently, the lithology types encountered at the Hydrite site are more heterogeneous including sandstones with variable grain size, mineralogy, and amounts of subordinate clay and silt, shales, siltstones, and dolostones.

A triple tube coring system was used with a coring diameter of 2.4 in (6.1 cm) (i.e., HQ3) at both sites. Two boreholes were cored at Santa Susana site, designated RD109 and C3. At Hydrite site, two boreholes were again cored, designated MP24S and MP25S. Cores were preserved to retain moisture content and reduced exposure to oxygen on site and sent to the laboratory for subcoring to a diameter of 3.8 cm. Smaller rock samples were subsampled at the same depths as the subcores, such that physical measurements could be collected and compared on colocated samples.

At Santa Susana site, 11 subcores were prepared from borehole RD109 over approximately a 105 m interval (30–135 m below ground surface (bgs)) and 11 subcores were prepared from borehole C3 over approximately a 35 m interval (7–42 m bgs). At Hydrite site, five horizontal subcores (designated 2H in Table 1) and seven vertical subcores (designated 1V in Table 1) were prepared from borehole MP24S over a 20 m interval between 34 and 54 m bgs. Four horizontal subcores and five vertical subcores were prepared from borehole MP25S over an approximately 14 m interval from 40 to 54 m bgs. Within this paper, horizontal and vertical subcores at Hydrite site were considered independent samples such that this analysis does not consider any effects of anisotropy.

Klinkenberg corrected (Klinkenberg, 1941) gas permeability was measured on the subcores. The subcores were saturated by applying a vacuum to at least 5×10^{-2} mbar, adding the saturating fluid, and then applying 34.5 bar (500 psi) for 20 min. The fluid was boiled and infused with nitrogen gas prior to saturation

Table 1
Physical Properties and CC Parameters for Samples

Sample name	Rock type and/or formation location	Physical properties				CC parameters					
		S_{por} (μm^{-1})	l_c (μm)	Permeability (m^2)	Porosity (%)	σ_w (mS/m)	F (–)	σ''_{1Hz} (mS/m)	m_n (mS/m)	τ_{pc} (s)	τ_{mean} (s)
Hydrite (new)											
MP24S-P-001-1V	Tonti Mbr./Sandstone	14.05	15.92	5.37E-15	11.8	66.5	44.0	0.102	0.820	2.151	0.771
MP24S-P-002-1V	Tonti Mbr./Sandstone	3.23	21.37	6.12E-14	16.2	66.5	26.4	0.014	0.169	0.518	0.349
MP24S-P-002-2H	Tonti Mbr./Sandstone	3.92	21.37	2.46E-13	13.5	66.5	30.8	0.011	0.110	0.652	0.057
MP24S-P-003-1V	Readstown Mbr./Sandstone	19.08	14.25	7.82E-15	12.9	66.5	38.1	0.083	0.676	3.460	0.599
MP24S-P-003-2H	Readstown Mbr./Sandstone	22.67	14.25	1.76E-14	11.1	66.5	49.8	0.079	0.655	2.151	0.774
MP24S-P-004-1V	Readstown Mbr./Sandstone	2.28	20.99	3.26E-13	18.3	66.5	16.8	0.034	0.347	0.518	0.295
MP24S-P-004-2H	Readstown Mbr./Sandstone	2.63	20.99	3.62E-13	16.3	66.5	20.4	0.008	0.077	0.733[a]	0.082
MP24S-P-005-1V	Lone Rock Fm./Sandstone	78.45	4.13	1.72E-16	19.3	66.5	19.6	0.226	1.627	1.337	0.480
MP24S-P-006-1V	Lone Rock Fm./Shaley Sandstone	67.21	8.19	1.56E-15	22.4	66.5	16.5	0.138	1.057	2.151	1.281
MP24S-P-006-2H	Lone Rock Fm./Shaley Sandstone	86.03	8.19	6.43E-15	18.5	66.5	19.6	0.133	1.125	2.151	0.378
MP24S-P-007-1V	Lone Rock Fm./Sandstone	69.08	22.18	3.37E-16	19.2	66.5	23.4	0.071	0.699	3.460	1.724
MP24S-P-007-2H	Lone Rock Fm./Sandstone	62.95	22.18	6.23E-14	20.6	66.5	15.0	0.103	0.986	2.151	0.868
MP25S-P-001-1V	St. Peter Fm. material infilling a Prairie du Chien karst channel/Sandstone	20.55	5.38	5.72E-15	22.3	66.5	20.8	0.112	1.070	1.501[a]	0.047
MP25S-P-001–2H	St. Peter Fm. material infilling a Prairie du Chien karst channel/Sandstone	22.22	5.38	5.87E-15	21.1	66.5	22.7	0.114	1.102	1.153[a]	0.111
MP25S-P-002-1V	St. Lawrence Fm./sandy Dolostone	81.58	0.63	9.21E-17	12.6	66.5	45.4	0.053	0.576	0.228[a]	0.243
MP25S-P-002-2H	St. Lawrence Fm./sandy Dolostone	73.55	0.63	1.78E-16	13.8	66.5	33.4	0.062	0.674	0.217[a]	0.054
MP25S-P-003-1V	St. Lawrence Fm./sandy Dolostone	50.84	0.84	1.38E-14	15.6	66.5	38.4	0.042	0.443	0.078[a]	0.270
MP25S-P-003-2H	St. Lawrence Fm./sandy Dolostone	52.08	0.84	4.01E-15	15.3	66.5	34.6	0.063	0.678	0.221[a]	0.325
MP25S-P-004-1V	Lone Rock Fm./Shaley Sandstone	78.75	4.16	1.02E-15	16.3	66.5	27.4	0.112	0.988	2.151	0.701
MP25S-P-004-2H	Lone Rock Fm./Shaley Sandstone	81.35	4.16	7.83E-16	16.0	66.5	27.1	0.059	0.563	1.337	0.331
MP25S-P-006-1V	Lone Rock Fm./Sandstone	64.21	17.78	5.43E-15	21.6	66.5	14.6	0.130	1.344	5.488	1.944
Santa Susana (new)											
C3-Cl-100.0	Sandstone	47.05	6.56	1.89E-15	14.1	66.5	50.1	0.195	1.350	0.518	0.243
C3-Cl-118.6	Sandstone	25.69	8.19	7.39E-15	14.9	66.5	38.9	0.171	1.287	0.323	0.327
C3-Cl-139.7	Sandstone	34.48	4.90	1.31E-15	15.6	66.5	46.5	0.201	1.737	2.151	0.578
C3-P-015	Sandstone	22.15	6.56	4.55E-15	13.1	66.5	51.0	0.159	1.304	0.049	0.177
C3-P-019	Sandstone	21.40	6.21	3.73E-15	14.6	66.5	45.1	0.218	1.729	0.126	0.209
C3-P-021	Sandstone	29.40	3.54	7.93E-16	14.2	66.5	50.8	0.204	1.471	0.078	0.104
C3-P-022	Sandstone	51.19	12.05	2.71E-15	10.1	66.5	50.9	0.221	1.904	0.019	0.214
C3-P-023	Sandstone	36.92	4.90	4.96E-16	12.9	66.5	46.6	0.263	2.052	0.049	0.159
C3-P-024	Sandstone	43.57	3.90	1.80E-15	13.1	66.5	39.7	0.234	1.757	0.126	0.102
C3-P-027	Sandstone	12.05	9.15	1.47E-14	13.3	66.5	40.2	0.063	0.509	0.078	0.061
C3-P-037	Sandstone	18.70	8.19	7.54E-15	13.7	66.5	51.4	0.162	1.267	0.078	0.146
C3-P-038	Breccia	36.65	4.90	8.62E-16	12.5	66.5	59.6	0.183	1.398	0.126	0.130
C3-P-040	Sandstone	25.93	6.21	1.84E-15	14.0	66.5	47.6	0.196	1.542	0.126	0.180
RD109-GEO-01	Sandstone	29.60	7.75	1.10E-14	14.1	66.5	27.2	0.291	2.098	0.078	0.144
RD109-GEO-06	Interbedded Sandstone/Siltstone	40.71	2.43	1.73E-15	15.4	66.5	32.1	0.255	1.594	0.126	0.125
RD109-GEO-14	Sandstone	25.48	7.75	3.33E-15	16.0	66.5	37.6	0.306	2.097	0.201	0.240
RD109-GEO-16	Sandstone	24.28	6.56	5.88E-15	16.6	66.5	39.5	0.294	2.010	0.126	0.172
RD109-P-01	Sandstone	21.50	6.21	3.90E-15	16.7	66.5	30.5	0.246	1.712	0.049	0.109
RD109-P-02	Sandstone	25.41	4.36	1.61E-15	14.5	66.5	44.6	0.230	1.623	0.078	0.138
RD109-P-03	Sandstone	25.60	6.93	7.52E-15	15.1	66.5	38.5	0.241	2.037	0.323	0.973
RD109-P-05	Sandstone	27.87	5.63	5.17E-15	13.1	66.5	46.6	0.264	2.182	0.126	0.144
RD109-P-06	Sandstone	22.11	8.65	1.11E-15	13.2	66.5	49.7	0.271	2.299	0.030	0.233
Chinese sandstones—Zhang and Weller (2014)											
CS-1	Shahejie	48.43	0.35	1.27E-16	12.5	100	46.7	0.139	0.736	0.063	0.104
CS-3	Shahejie	12.15	7.36	2.47E-14	17.0	100	26.5	0.201	1.071	0.798	0.346
CS-5	Shahejie	7.36	9.80	4.51E-14	16.3	100	28.7	0.109	0.684	1.592	0.415
CS-14	Shahejie	20.92	5.45	5.88E-15	16.9	100	26.9	0.222	1.223	1.004	0.620
CS-18	Shahejie	4.57	8.40	2.33E-14	16.9	100	26.8	0.106	0.595	0.798	0.248
Egyptian sandstones— Abuseda et al. (2016)											
7H1	Bahariya	2.73	13.04	5.06E-14	18.1	100	20.0	0.131	1.128	6.336	0.947
18H1	Bahariya	15.74	6.69	1.06E-14	17.0	100	16.1	0.273	1.803	1.264	0.305

Table 1. (continued)

Sample name	Rock type and/or formation location	Physical properties				CC parameters					
		S_{por} (μm^{-1})	l_c (μm)	Permeability (m^2)	Porosity (%)	σ_w (mS/m)	F (–)	σ''_{1Hz} (mS/m)	m_n (mS/m)	τ_{pc} (s)	τ_{mean} (s)
22H	Bahariya	37.81	5.17	3.53E-15	16.5	100	27.9	0.268	1.599	1.004	0.476
28H1	Bahariya	1.34	8.41	6.74E-14	19.8	100	22.1	0.036	0.246	1.592	0.249
43H1	Bahariya	2.49	16.27	1.12E-13	23.7	100	12.5	0.126	0.948	2.522	0.451
53H2	Bahariya	3.89	14.65	1.14E-13	23.1	100	13.1	0.114	0.806	2.522	0.314
55	Bahariya	19.66	10.68	1.01E-13	22.8	100	14.5	0.320	1.429	0.798	0.416
Other											
BH6	Bentheimer	4.12	35.72	4.20E-13	21.7	100	11.9	0.053	0.360	0.126	0.144
ES-14	Elb-sandstone	1.06	31.75	2.84E-12	23.0	100	18.7	0.094	0.525	0.217	0.301
GR1	Green sand	31.33	36.26	3.26E-13	24.0	100	11.7	0.292	1.365	3.475	0.215

[a]A corner value of τ was used for this sample.

to minimize air bubbles within the pores. Gravimetric porosity was calculated from the mass difference between saturated and dry subcores divided by submersible volume. MICP (up to 2,068 bar/30,000 psi), nitrogen-gas BET and X-ray diffraction (XRD) data were acquired on the colocated smaller samples and used to determine specific surface area and mineralogical composition, respectively.

CC measurements were collected on subcores saturated first with a low salinity solution and subsequently with a high salinity solution. The low salinity solution contained calcium chloride and magnesium sulfate in concentrations similar to the site groundwater and had a fluid conductivity of 66.5 mS/m. The high salinity solution was a sodium chloride solution with a fluid conductivity of 8 S/m. The CC measurements of subcores saturated with the high salinity solution were used to determine the electrical formation factor F.

CC measurements were acquired using sample holders designed, tested, and calibrated following the procedure in Kemna et al. (2012) to remove measurement artifacts that can occur due to the electrode positions. A Portable Spectral-Induced Polarization (PSIP) instrument (Ontash & Ermac Instruments, NJ, USA) recorded CC over a frequency range of 10^{-3}–10^{3} Hz, with five measurements per decade of frequency, for a total of 36 measurements. To avoid errors due to temperature fluctuations, the measurements were collected on sample holders placed in an environmental chamber set to 25°C. To ensure equilibration of temperature and ion exchange processes between the saturating pore fluid and mineral surface, measurements were collected twice daily (for approximately 1 week) until the difference between a previously collected measurement of both the resistance and phase was less than 2%; data collected at 1 Hz were used to quantitatively compare successive measurements, but the entire spectrum was visually inspected for consistency. Resistance and phase data were converted to complex conductivity using the geometric factor for the sample holder, which was experimentally determined from measurements on water samples of precisely known complex conductivity.

3.2. Previously Published Samples

We supplement this extensive new data set with 15 samples from multiple sources including: five Eocene sandstone samples of the Shahejie Formation (CS samples, China) (Zhang & Weller, 2014), seven samples of the Cretaceous Bahariya Formation (Egypt) (Abuseda et al., 2016), and three unpublished samples from various locations in Germany (Bentheimer, Elbe-sandstone, Green sand). Physical and geophysical measurements were available for our analysis including BET derived S_{por}, permeability, F, and CC spectra.

3.3. Analysis of the CC Spectra

A characteristic relaxation time is typically used to represent CC data. Here we used two characteristic τ values: τ_{mean}, which is calculated from Debye decomposition and takes into account the entire CC spectrum, and τ_{pc} which is associated with a characteristic frequency f_{char}. Since different behaviors can be observed in the CC spectrum, the procedure to choose f_{char} can vary (Revil et al., 2015; Schwarz, 1962). Within our sample database, the σ'' spectra exhibited either a well-defined peak frequency f_p or a corner frequency f_c where σ'' rapidly decreased toward lower frequencies (Revil et al., 2015). If the σ'' spectrum contained a well-defined peak frequency, a parabola was fit to the five data points centered on this peak and used to

estimate the apex, equal to f_p. If there was no clear peak, a spline was fit to the data points and f_c was chosen as the intersection of two linear fits to the data following the method of Revil et al. (2015). The time constant was then calculated from $\tau_{pc}=1/2\pi f_{pc}$, where p or c indicates either peak or corner. Examples of peak and corner selection for two samples are shown in supporting information Figure S1.

To compare the predictive capabilities of the different models, the average absolute logarithmic deviation between predicted parameters, p^* and measured parameters p was determined by:

$$d=\frac{1}{n}\sum_{j=1}^{n}|\log_{10}p_j-\log_{10}p_j^*|, \tag{12}$$

where d represents the average, or mean absolute deviation on a logarithmic scale. A d value equal to 1 indicates that the average misfit between the predicted data point and the measured parameter is one order of magnitude. In regards to permeability model estimates, one order of magnitude above or below measured values (i.e., $d = 1.0$) is commonly considered to yield an acceptable estimation.

4. Results

Table 1 summarizes all physical properties and CC parameters for the 58 samples used in this study. Permeability ranges from 9.21 $\times$ 10^{-17} to 2.84 $\times$ 10^{-12} m^2 (0.0933–2,875 mD), spanning more than four orders of magnitude. The other physical properties also demonstrate the variation in the pore geometry among these sandstones: porosity ranges from 10.1% to 24.0%; F ranges from 11.7 to 59.6; S_{por} ranges from 1.06 to 86.03 μm^{-1}. We report σ'' at a frequency of 1 Hz to facilitate direct comparison with previous studies (Weller et al., 2010, 2015a, 2015b).

4.1. PaRiS and Katz-Thompson (KT) Geometric Models

We first test the predictions of the PaRiS model (equation (4)) and KT model using 0.19 $l_c/2=\Lambda$ in (equation (6)) based on the geometric length scales, $1/S_{por}$ and Λ, respectively (Figure 2). As we are only interested in examining the predictive capabilities of these models in a field setting, no effort has been made to optimize the coefficient or scaling constants in the equations. The 1:1 line is shown as a solid line in Figure 2 and the dashed lines represent one order of magnitude of variation above and below the 1:1 line.

The colorscale of the data points represents S_{por} and highlights the general trend of a decrease in measured permeability with an increase in S_{por}. Using the PaRiS model (Figure 2a), permeability of the high S_{por} samples is underpredicted, with several data points deviating by more than one order of magnitude. The permeability of several low S_{por} samples is overpredicted.

Using the KT model (Figure 2b), most permeabilities are underpredicted but fall within one order of magnitude of the actual measured values. Based on the d values, the KT model (equation (6) using Λ) ($d = 0.729$) yields a better prediction of permeability than the PaRiS model ($d = 1.023$).

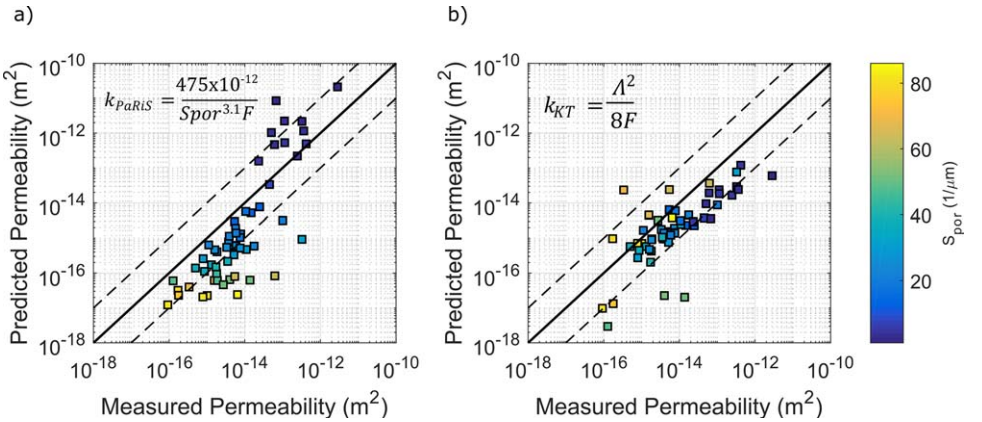

Figure 2. Permeability predictions using geometric length scales (a) PaRiS model per equation (4) ($d = 1.023$) and (b) KT model with Λ per equation (6) ($d = 0.729$).

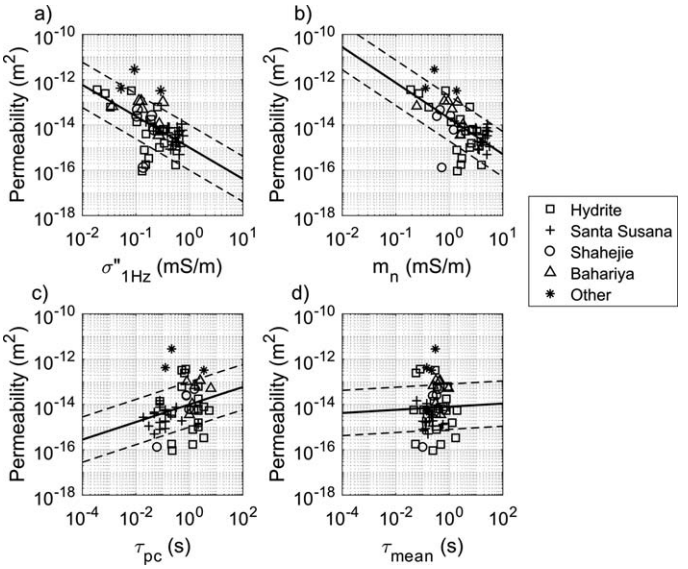

Figure 3. Measured permeability versus CC parameters plotted on a logarithmic scale: (a) σ''_{1Hz}, (b) m_n, (c) τ_{pc}, and (d) τ_{mean}. Regression (solid black) lines show the fitted power law relation. Dashed lines show plus or minus one order of permeability magnitude.

4.2. Equivalent Geophysical Length Scale Models

4.2.1. Dependence of CC Measurements on Geometric Properties

Relationships between CC parameters (σ''_{1Hz}, m_n, τ_{pc}, τ_{mean}) and measured permeability are shown in Figure 3. Since σ''_{1Hz} and m_n are sensitive to salinity (i.e., c_p depends on fluid chemistry) (Niu et al., 2016; Revil & Skold, 2011; Weller & Slater, 2012) data from the Santa Susana and Hydrite samples were corrected to a fluid conductivity σ_f of 100 mS/m using $\sigma''(\sigma_f)=C_f\sqrt{\frac{\sigma_f}{\sigma_w}}\sigma''(\sigma_w)$ (Weller et al., 2015a, equation (17)). C_f was set equal to 2, to account for the calcium chloride, and σ_w was set equal to the conductivity of the saturating fluid (i.e., 66.5 mS/m) resulting in a value of $\sqrt{\frac{\sigma_f}{\sigma_w}}=1.23$. A linear regression was applied to the logarithmic CC parameters versus permeability to determine the coefficients for a power law relationship of the form $k=aX^b$ (with X equal to σ''_{1Hz}, m_n, τ_{pc}, τ_{mean}). The b values are given in Table 2. These plots show the expected trends: permeability decreases with increasing σ''_{1Hz} and m_n; and permeability increases with increasing τ_{pc} and τ_{mean} (based on regression exponents presented in Table 2). The relationship between F and permeability is shown in Figure 4. Similar to Figure 3, a linear regression on the logarithmic values was used to determine the coefficients for a power law relationship between F and measured permeability. The relationship between F and measured permeability shows, as expected, that measured permeability decreases with F (Figure 4).

4.2.2. Polarization Magnitude Geophysical Models

Predictions of permeability for the polarization magnitude geophysical models are shown in Figure 5. Permeability is well-predicted (within one order of magnitude) from equations (7) and (8) (Figure 5) with the exception of samples with a high S_{por} (>60 μm^{-1}) (see Table 1). The d values for the polarization magnitude geophysical models demonstrate less than within one order of magnitude misfit for single frequency (σ''_{1Hz}) (0.770) versus multifrequency (m_n) (0.807) CC parameters (Table 3). The polarization magnitude geophysical models are a better predictor of permeability than the PaRiS model (equation (4)) based on d misfit alone (1.023 versus values stated above) (Table 3).

A single value of c_p (as in equations (7) and (8)) may not represent all samples, contributing to the poor prediction of permeability for the high S_{por} samples. Applying a linear least squares regression to σ''_{1Hz} versus S_{por} yields an optimal c_p value of 4.9×10^{-10} S, although the coefficient of determination is low ($R^2 = 0.40$). In contrast, individually calculating c_p for each sample shows a large range of potential c_p values based on the mean of 16.7×10^{-12} S and standard deviation of 14.5×10^{-12} S (maximum = 88.9×10^{-12} S, minimum = 1.6×10^{-12} S).

4.2.3. Time Constant Geophysical Model

Permeability predictions from equation (11) using the time constants τ_{pc} and τ_{mean} with F directly determined from the high salinity data are shown in Figures 6a and 6b, respectively. A single value of D_+ equal to 3.8×10^{-12} m^2/s (clayey-sand) was assumed since our samples are best represented as clayey sandstones rather than clean sandstones. Permeability is well-predicted (within one order of magnitude) again with the exception of the samples with high S_{por} (>60 μm^{-1}). In addition, a few low S_{por} are also outliers. Figure 6 demonstrates that the overall predictions of k are similar when using either τ_{pc} or τ_{mean} (Table 3).

A complicating factor in the use of equation (11) to calculate k, is determining an appropriate value of D_+. If the two proposed values of 1.3×10^{-9} m^2/s for clean sands and 3.8×10^{-12} m^2/s for clayey material (Koch et al., 2011; Revil, 2013; Revil et al., 2012) best represent D_+ values for all samples, then by rearranging equation (11), the values of log $4Fk$ plotted versus log τ_{pc} should fall on two distinct lines, the slopes of which corresponds to D_+. However, as seen in Figure 7a, this is not the case; there is a large scatter in this plot and the samples do not consistently fall along either line similar to the observations of

Table 2
Power Law Exponents, b, Resulting From Least Squares Regression of Logarithmic Geophysical Parameters Versus Permeability

Parameter	b
σ''_{1Hz}	−1.4
m_n	−1.6
τ_{pc}	0.4
τ_{mean}	0.1
F	−2.8

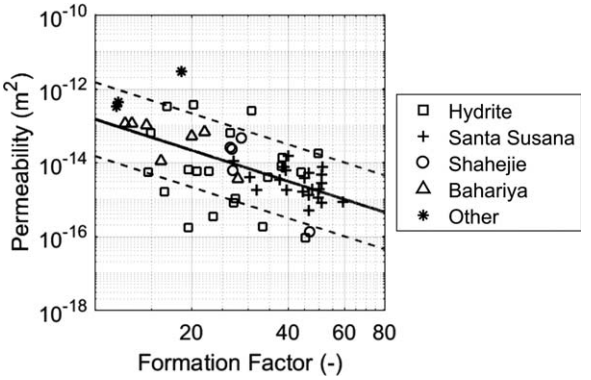

Figure 4. Measured permeability versus F plotted on a logarithmic scale. Regression (solid black) line show the fitted power law relation. Dashed lines show plus or minus one order of permeability magnitude.

Weller et al. (2016). The large scatter indicates a wide range of D_+ which does not appear to be associated with individual formations.

By calculating individual values of D_+ for each sample, using equation (11) and the known values for F, k, and τ_{pc}, we can group the samples and determine a more appropriate value of D_+. From Figure 7b, higher S_{por} samples are better represented by a lower D_+ and lower S_{por} samples are better represented by a higher D_+. We thus define three linearly spaced groups of samples based on the values of S_{por} (0–29 μm^{-1}; 30–57 μm^{-1}; 58–86 μm^{-1}) and calculate D_+ for each group. The values for D_+ determined from this approach are: 4.96×10^{-12} m^2/s for the low S_{por} samples, 2.13×10^{-12} m^2/s for the midrange S_{por} samples and 6.98×10^{-14} m^2/s for the high S_{por} samples. The new lines representing these D_+ values are plotted alongside the data in Figure 7b. Using these new S_{por}-specific D_+ values, the permeability was predicted from equation (11); the results from the updated permeability model are shown versus the measured permeability in Figure 8. Unsurprisingly, using these S_{por}-specific D+ values improves the permeability prediction relative to using a single assumed value of D_+ alone. However, some outliers are not reconcilable using such variations in D_+.

5. Discussion

We have performed a first-of-a-kind comparative analysis of two recently proposed approaches to permeability prediction on 58 sandstone samples using geophysical lengths scales that can be defined from complex conductivity data and analyzed the uncertainty in these predictions that can be partly attributed to the variation in the electrochemical parameters D_+ and c_p. We have also evaluated permeability predictions from "as-is" geophysical length scales against predictions from geometric length scales. Using the geometric length scales $1/S_{por}$, and Λ in these formulations, permeability is reasonably predicted (Figure 2), although the coefficients in the PaRiS model (Figure 2a) are not optimal values for our database. The geophysical length scales c_p/σ''_{1Hz} and c_p/m_n (equations (7) and (8); Figure 5) and $\tau_{pc}D_+$ and $\tau_{mean}D_+$ (equation (11); Figure 6) were shown to provide estimates of permeability to within one order of magnitude for most samples. In general, the geophysical length scale models perform as well as the geometric length scale permeability models based on analysis of residuals (Table 3). Amongst the geophysical permeability models, the τ_{mean}-based model performs best relative to τ_{pc}, σ''_{1Hz}, and m_n models. Interestingly, all geophysical models outperform the PaRiS model based on the geometric length scale.

Many samples with high S_{por} appear as outliers in the geophysical length scale models while S_{por} does not have as large of an influence on outliers in the geometric length scale models. In the geophysical models

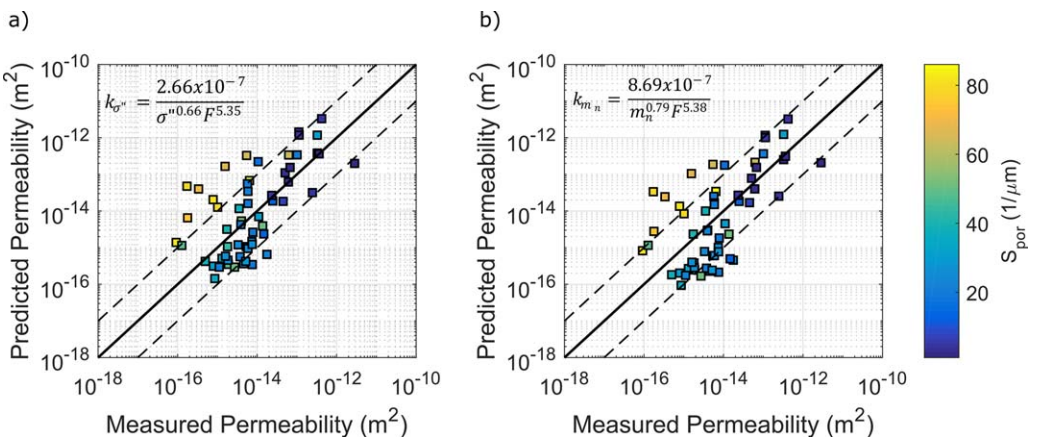

Figure 5. Permeability predicted for the polarization magnitude geophysical model using (a) σ''_{1Hz} (equation (7)) ($d = 0.770$) and (b) m_n (equation (8)) ($d = 0.807$).

Table 3
Summary d Misfits for Permeability Predictions Using Reference Equations

Key parameter type	Description	Equation	Eqn #	Figure #	*d* misfits	*d* misfits excluding samples where *Spor* >60
Geometric	PaRiS model	$k_{PaRiS}=\frac{475}{Spor^{3.1}F}$	4	2a	1.023	0.920
	Katz and Thompson (KT)-type	$k_{KT}=\frac{\Lambda^2}{8F}$	6	2b	0.729	0.746
Geophysical	Polarization magnitude σ''	$k_{\sigma''}=\frac{2.66\times10^{-7}}{\sigma''^{0.66}F^{5.35}}$	7	5a	0.770	0.611
	Polarization magnitude m_n	$k_{m_n}=\frac{8.69\times10^{-7}}{m_n^{0.79}F^{5.39}}$	8	5b	0.807	0.698
	Time constant τ_{pc}	$k_\tau=\frac{\tau_{pc}D_+}{4F}$	11	6a	0.779	0.480
	Time constant τ_{mean}	$k_\tau=\frac{\tau_{mean}D_+}{4F}$	11	6b	0.707	0.479
	Time constant τ_{pc} and $D_{+\,(Spor)}$	$k_\tau=\frac{\tau_{pc}D_{+\,(Spor)}}{4F}$	11	8	0.539	0.562

(Figures 5 and 6), permeability is overestimated for high S_{por} samples. The most likely cause of the permeability overestimation for high S_{por} samples is mineralogical variation and its associated impact on c_p and D_+. X-ray diffraction results show that high S_{por} samples are characterized by the presence of dolomite (Table 1), which might cause variations in c_p relative to quartz (Halisch et al., 2014) given that c_p accounts for the control of the interfacial chemistry and sample mineralogy on the polarizability. The high S_{por} samples containing dolomite (supporting information Figure S2) are interpreted to have a lower c_p than other samples which is similar to finding reported by Halisch et al. (2014) on carbonates. Similarly, these samples have a lower D_+ than the assumed single value for a clayey-sand (3.8×10^{-12} m^2/s).

Mineralogical variations may not be responsible for the overprediction of permeability in high S_{por} samples in the polarization magnitude geophysical model. One alternative possibility is that the calibration parameters in this model cause this effect, e.g., if the power law exponent on σ'' is too low. To assess this possibility, a multilinear regression using the form of equation (7) was performed to solve for the numerator and the σ'' and F exponential coefficients (supporting information Figure S3b). For the 58 samples in this database, it was found that the σ'' exponential coefficient increased only slightly from 0.66 to 0.96. Additionally, high S_{por} samples still appear as outliers, suggesting a structural and/or mechanistic behavior in these sandy dolostones that differs from other samples in our database. Interestingly, calibrating the coefficients in the polarization magnitude geophysical model (equation (7)) results in a slightly better d value ($d = 0.515$) than the calibration of equation (11) using the S_{por}-specific D_+ coefficients ($d = 0.539$).

To further assess the impact of mineralogical variability on permeability prediction, d values were calculated for all reference equations by omitting samples with high S_{por} (>60 μm^{-1}) (Table 3). Residuals for permeability predictions using geometric parameters S_{por} and Λ remain fairly constant, with a slight improvement

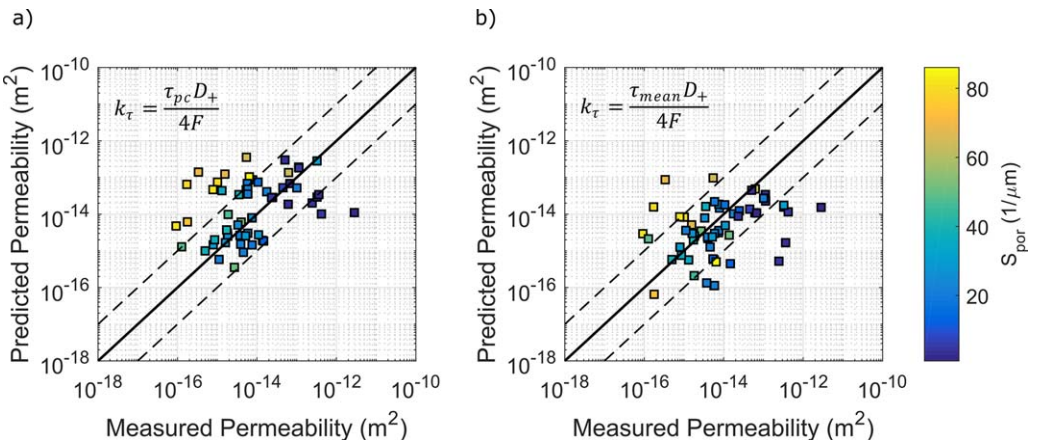

Figure 6. Permeability predicted from the time constant geophysical model (equation (11)) using (a) τ_{pc} (d=0.779) and (b)τ_{mean} (d=0.707)($D_+ = 3.8 \times 10^{-12}$ m^2/s).

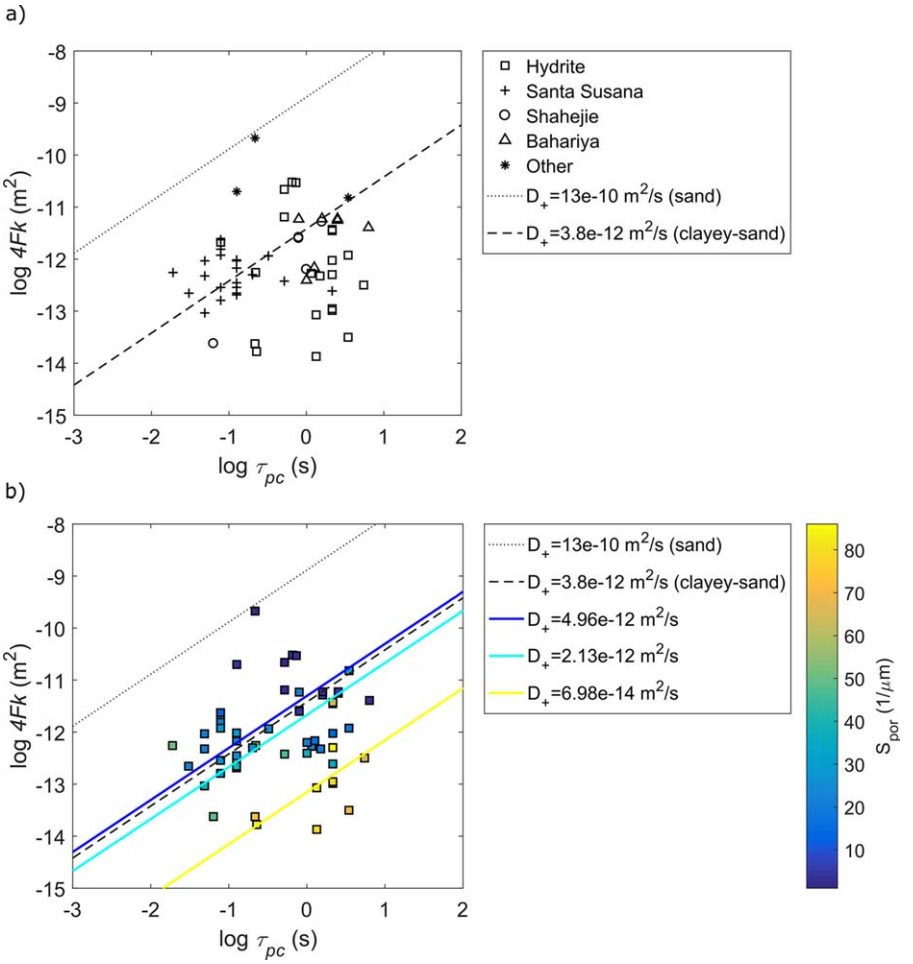

Figure 7. (a) Individual diffusion coefficients (D_+) for the sample database in Table 1 classified by lithological unit. Predicted values of $D_+ = 3.8 \times 10{-}12$ m^2/s for clayey-sand and $D_+ = 13 \times 10^{-10}$ m^2/s for clean sands are shown by dashed and dotted lines respectively. (b) Same as Figure 7a with S_{por} designated by the legend color scale. Binning samples by S_{por} into three groupings and solving for the best fit D_+ results in the three values shown (blue, cyan, and yellow lines).

in the PaRiS model and a slight decrease in for the KT-type model. All predictions using geophysical parameters τ_{pc}, τ_{mean}, σ''_{1Hz}, and m_n improve, with the largest improvement in the k_τ models not using an S_{por}-specific D_+. Integration of lithological information in geophysical permeability models could provide an improvement over existing models.

What explains a smaller c_p and D_+ for our samples containing dolomite? Weller et al. (2016) suspect that, for samples with increasing clay content and increasing specific surface area, a decrease in the ion mobility results in a smaller D_+. They suppose a stronger binding of ions at the surfaces dominates the diffusion in smaller pores associated with clay minerals, thereby reducing mobility. Similar to samples with high clay content, the high S_{por} in these sandy dolostones may be reducing the effective ionic mobility β^s_+, thereby reducing D_+. In regards to smaller c_p values in the sandy dolostone samples, the higher intracrystalline pore space (inferred from high S_{por} measured in these samples) may be weakly polarized relative to silicates. Alternatively, smaller c_p values may be attributed to the pH dependency of the CC response, specifically the difference in the point of zero charge (PZC) for dolomite versus silica. For Berea sandstones Lesmes and Frye (2001) found a reduced σ'' response at pH = 3, which corresponds to the PZC for silica; Skold et al. (2011) found a similar pH dependence for silica sands. In contrast, we compare the PZC of calcite, which has similar values to dolomite (Pokrovsky et al., 1999). The PZC of calcite has been reported within the pH range of 8–9.5 (Heberling et al., 2011; Somasundaran & Agar, 1967). Our CC data collection was performed at near neutral pH, i.e., much closer to the PZC for calcite relative to the PZC for silica. The σ'' would then

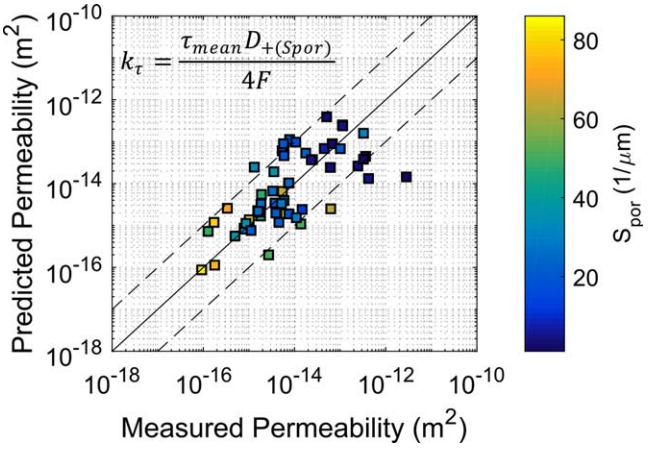

Figure 8. Using the time constant geophysical model (equation (11)) to solve for predicted permeability with three discrete values of D_+ defined based on S_{por} (Figure 7b). τ_{pc} is used as the time constant.

presumably be reduced for calcite when compared to silicates. However, several researchers have suggested that pH has no direct influence of electrical surface properties in calcites, but rather can be used to determine speciation of Ca^{2+} and CO_3^{2-}, which are the potentially determining ions (Amankonah et al., 1985; Foxall et al., 1979; Thompson & Pownall, 1989). While we suggest that the PZC plays a role in the reduced c_p for the sandy dolostone samples, the mechanisms clearly need further study.

A major limiting factor in the application of both the geometric and geophysical length scale k models is the use of the formation factor F. Since F is not directly measurable from borehole electrical logging or electrical imaging surveys, the application of these models to field-scale data is limited. We observe that k has a strong dependence on F (Figure 4), and so its inclusion in the permeability models is important. One solution to this limitation is to estimate F from electrical parameters that can be measured in the field. For instance, the predicted electrical formation factor F_p can be estimated from the real conductivity (σ') if σ_w is known (i.e., $F_p = \sigma_w/\sigma'$). This estimation assumes that the surface conduction is small, a questionable assumption even in relatively clean sands. In our database, F is underestimated by F_p for all but two samples (Figure 9a, d = 0.558).

In order to overcome this critical limitation of electrical measurements for permeability estimation, Borner et al. (1996) first suggested that F_p can be calculated as

$$F_p = \frac{\sigma_w}{\sigma' - \sigma'_{surf}} \cong \frac{\sigma_w}{\sigma'' - \frac{\sigma''}{l}} \tag{13}$$

where l is a linear coefficient that is assumed to relate σ'' to the real part of the surface conductivity (σ'_{surf}). Borner et al. (1996) suggested l ranges between 0.01 and 0.15. More recent studies on larger databases have found $l = 0.042$ ($R^2 = 0.91$) (Weller et al., 2013) or $l = 0.037$ ($R^2 = 0.79$) (Revil et al., 2015) for sandstone samples. Based on the 58 samples in this study, the linear least squares regression gives $l = 0.044$ ($R^2 = 0.75$). We use $l = 0.042$ (Weller et al., 2013) to calculate F_p for the 58 sandstone samples without any model calibration. This improves the prediction of F relative to using $F_p = \sigma_w/\sigma'$ although F_p still mostly underpredicts true F (Figure 9b, $d = 0.403$). Using $l = 0.044$, the prediction improves slightly (Figure 9c, $d = 0.336$). The impact of an incorrect estimate of F on the permeability prediction depends in part on the relative weighting of F in the models. For example, in the geophysical polarization magnitude equation given by equations (7) and (8), F is raised to the power 5.35 and 5.38, respectively, resulting in large deviations from true permeability values when F is in error. In contrast, F is only raised to the power 1 in the geophysical time constant model (equation (11)). In these models, deviations from the true permeability do not increase so markedly when F_p is used in place of F.

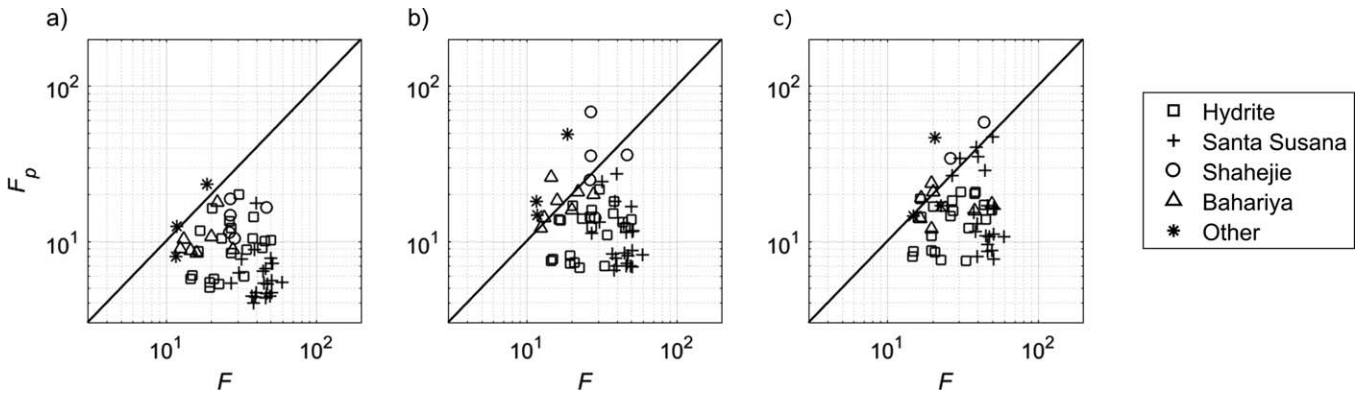

Figure 9. Predicted electrical formation factor F_p versus measured formation factor F where (a) $F_p = \sigma_w/\sigma'$ ($d = 0.558$), (b) F_p is calculated from equation (13) using $l = 0.042$ ($d = 0.403$) (Weller et al., 2013) and (c) F_p is calculated from equation (13) using $l = 0.044$ ($d = 0.336$).

The selection of σ''_{1Hz} in the polarization magnitude model (equation (7)) is arbitrary and primarily based on facilitating integration of a large number of independently determined data sets into model calibration (Weller et al., 2015a). To evaluate the effect of this choice on the permeability estimates, a sensitivity analysis was performed to quantify variations in d as a function of measurement frequency when permeability prediction is based on equation (7) (supporting information Figure S4). Permeability is predicted to within one order of magnitude regardless of the frequency at which σ'' is selected and the variability of d is small (0.757–0.788). In fact, the 1 Hz frequency has the median d value, suggesting that permeability would be slightly better predicted at some other frequencies.

Field-based acquisition of CC parameters is increasing with the advent of new instrumentation and measurement techniques (Kemna et al., 2014; Slater et al., 2018). Considering the impracticality of applying the geometric permeability models in the field, the geophysical models might provide a solution to field-scale estimation of permeability. This study has highlighted that opportunity, as noted by the fact that the geophysical length scale in the polarization magnitude model provides a better prediction of permeability than the geometric length scale in the PaRiS model. However, significant challenges remain with the CC-based estimation of permeability. First and foremost is the limitation that F is not readily measurable at the field scale. Beyond this, each geophysical model has limitations. In the polarization magnitude geophysical model (equations (7) and (8)), variations in fluid chemistry, are accounted for within c_p whereas such factors control D_+ in the geophysical time constant model (equation (11)). Representative values of these parameters must be assumed for field-scale implementation of the models. Unsurprisingly, an improvement was seen in the time constant model with the application of three S_{por}-specific D_+ values (Figure 8 and Table 3). However, the diffusion coefficients will be unknown in the field, so this is not a practical approach to improving model performance. For our 58 samples, S_{por}-specific D_+ values vary by two orders of magnitude. In contrast, the majority of individual c_p values vary by less than one order of magnitude. All other factors being equal, permeability prediction on high S_{por} samples using the time constant geophysical model with a single value of D_+ would be more uncertain relative to polarization magnitude models utilizing a single c_p value.

While CC data acquisition is increasing at the field scale, it is currently very challenging to acquire reliable broadband frequency spectra. In contrast, it is relatively straightforward to measure a single frequency σ'' and much less time consuming. All geophysical parameters used (i.e., m_n,τ_{pc}, and τ_{mean}) except σ'' necessitate collection of multifrequency data, with not much improvement in permeability prediction (Table 3). In addition, not all CC spectra indicate a peak frequency and the nonprescriptive selection of τ_{pc} in the time constant geophysical model adds further uncertainty to this approach, as there are several ways in which to estimate this parameter. These observations support the use of σ'' to estimate permeability at the field scale from electrical measurements.

This study explored the predictive capability of previously proposed PaRiS, KT-type, polarization magnitude, and time constant permeability models that utilize geometric and geophysical length scales. Limitations of the models, specifically with respect to field-scale applications, were considered. The primary limitation of all investigated models is the requirement of a reliable estimate of F, particularly where F has a strong influence on the model. This is particularly evident in the polarization magnitude permeability models (equations (7) and (8)) where uncertainty in F will result in large prediction errors due to the large power law exponents of 5.35 and 5.38. While this limitation has yet to be overcome in low salinity groundwater settings, the models are expected to perform well in (1) brine formations where F can be reliably measured in the field assuming that the brine conductivity is known and low phase angles can be measured under field conditions and (2) where surface conduction effects are very low. Future work will explore permeability estimation from geophysical length scales in such high salinity (i.e., brine) and low surface conduction formations.

6. Conclusions

Complex conductivity offers the possibility of field-scale permeability prediction through the measurement of geophysical length scales analogous to geometric length scales. Permeability for most samples from an extensive database of sandstones can be predicted to within one order of magnitude from previously proposed CC models based on either a polarization magnitude or a time constant. Exceptions are samples characterized by high S_{por} and mineralogical variability, particularly the presence of dolomite. The dependence of the geophysical length scales on mineralogical variability not captured in the use of single values

of a specific polarizability (c_p) or diffusion coefficient (D_+) may explain the limited predictive capability of these k estimation models. Several limitations to the geophysical permeability models have been identified including the time constraint imposed by the acquisition of multifrequency data in models using m_n, τ_{pc}, and τ_{mean}, the existence and selection of τ_{pc} in the covered frequency range and the large uncertainty in the appropriate value of a representative diffusion coefficient. However, the largest obstacle to the field-scale implementation of the permeability equations (both geometrical and geophysical) is a reliable estimation of electrical formation factor (F). A recently proposed method to estimate F based on a surface conductivity correction using CC measurements improves F predictions but still leaves significant errors in that will limit field-scale k estimation using such models.

Notation

CC	Complex conductivity (mS/m)
c_p	Specific polarizability (S)
d	Mean absolute deviation on a logarithmic scale
D_+	Diffusion coefficient (m^2/s)
F	Electrical formation factor (–)
k	Permeability (m^2)
k_{KT}	Modified Katz and Thompson permeability model (m^2)
$k_{\sigma''}$	Geophysical polarization magnitude permeability model from Weller et al. (2015a) using σ''_{1Hz} (m^2)
k_{m_n}	Geophysical polarization magnitude permeability model from Weller et al. (2015a) using m_n (m^2)
k_τ	Permeability model from Revil et al. (2012) using time constant τ_{pc} or τ_{mean} (m^2)
l_c	Equivalent pore diameter where maximum incremental intrusion occurs using MICP (μm)
Λ	Dynamically interconnected pore radius (μm)
MICP	Mercury injection capillary pressure
m_n	Normalized chargeability (mS/m)
r_{eff}	Effective hydraulic radius (μm)
S_{por}	Pore volume normalized surface area (μm^{-1})
τ	Time constant (s)
τ_{mean}	Time constant (s) obtained from a Debye decomposition
τ_{pc}	Peak and/or corner characteristic time constant (s)
σ''	Imaginary conductivity (mS/m)
σ''_{1Hz}	Imaginary conductivity (mS/m) at a frequency of 1 Hz

Acknowledgments
This material is based upon work supported by the U.S. Army Corps of Engineers, Humphreys Engineering Center Support Activity under contract W912HQ-14-C-0018. The Santa Susana and Hydrite site cores were obtained from coring activities funded by the site owners, The Boeing Corporation and Hydrite Chemical Corporation, respectively, in support of the University of Guelph G360 Institute research program. The samples were selected from the study boreholes with the experienced research scientists from Dr. Jessica Meyer and Amanda Pierce. The data used for this study are listed in Table 1. We thank Dr. Philippe Leroy, Dr. Andreas Hördt, and an anonymous reviewer for their comments which improved this manuscript.

References

Abuseda, H., Weller, A., Sattler, C., & Debschütz, W. (2016). Petrographical and petrophysical investigations of upper cretaceous sandstones of the South West Sennan field, Western Desert, Egypt. *Arabian Journal of Geosciences*, *9*, 1–18. https://doi.org/10.1007/s12517-015-2156-1

Amankonah, J. O., Somasundaran, P., & Ananthapadmabhan, K. P. (1985). Effects of dissolved mineral species on the dissolution/precipitation characteristics of calcite and apatite. *Colloids and Surfaces*, *15*, 295–307. https://doi.org/10.1016/0166-6622(85)80080-9

Amirtharaj, E. S., Ioannidis, M. A., Parker, B., & Tsakiroglou, C. D. (2011). Statistical synthesis of imaging and porosimetry data for the characterization of microstructure and transport properties of sandstones. *Transport in Porous Media*, *86*, 135–154. https://doi.org/10.1007/s11242-010-9612-x

Banavar, J. R., & Johnson, D. L. (1987). Characteristic pore sizes and transport in porous media. *Physical Review B*, *35*, 7283–7286. https://doi.org/10.1103/PhysRevB.35.7283

Binley, A., Hubbard, S., Huisman, J., Revil, A., Robinson, D., Singha, K., et al. (2015). Understanding of subsurface processes over multiple scales. *Water Resources Research*, *51*, 3837–3866. https://doi.org/10.1002/2015WR017016

Binley, A., Slater, L. D., Fukes, M., & Cassiani, G. (2005). Relationship between spectral induced polarization and hydraulic properties of saturated and unsaturated sandstone. *Water Resources Research*, *41*, W12417. https://doi.org/10.1029/2005WR004202

Borner, F. D., Schopper, J. R., & Weller, A. (1996). Evaluation of transport and storage properties in the soil and groundwater zone from induced polarization measurements. *Geophysical Prospecting*, *44*, 583–601. https://doi.org/10.1111/j.1365-2478.1996.tb00167.x

Carman, P. C. (1939). Permeability of saturated sands, soils and clays. *Journal of Agricultural Science*, *29*, 262. https://doi.org/10.1017/S0021859600051789

Foxall, T., Peterson, G. C., Rendall, H. M., & Smith, A. L. (1979). Charge determination at calcium salt/aqueous solution interface. *Journal of the Chemical Society, Faraday Transactions 1: Physical Chemistry in Condensed Phases*, *75*, 1034–1039. https://doi.org/10.1039/f19797501034

Guéguen, Y., & Palciauskas, V. (1994). *Introduction to the physics of rocks*. Princeton, NJ: Princeton University Press.

Halisch, M., Weller, A., & Kassab, M. A. (2014). Impedance spectroscopy on carbonates. In *Proceeding of the annual symposium of the Society of Core Analysis* (paper A036) Google Scholar 2014. Avignon, France.

Heberling, F., Trainor, T. P., Lützenkirchen, J., Eng, P., Denecke, M. A., & Bosbach, D. (2011). Structure and reactivity of the calcite-water interface. *Journal of Colloid and Interface Science*, *354*, 843–857. https://doi.org/10.1016/j.jcis.2010.10.047

Johnson, D. L., Koplik, J., & Schwartz, L. M. (1986). New pore-size parameter characterizing transport in porous media. *Physical Review Letters*, *57*, 2564–2567. https://doi.org/10.1103/PhysRevLett.57.2564

Katz, A. J., & Thompson, A. H. (1986). Quantitative prediction of permeability in porous rock. *Physical Review B*, *34*, 8179–8181. https://doi.org/10.1103/PhysRevB.34.8179

Katz, A. J., & Thompson, A. H. (1987). Prediction of rock electrical conductivity from mercury injection measurements. *Journal of Geophysical Research*, *92*, 599. https://doi.org/10.1029/JB092iB01p00599

Kemna, A., Binley, A., Cassiani, G., Niederleithinger, E., Revil, A., Slater, L., et al. (2012). An overview of the spectral induced polarization method for near-surface applications. *Near Surface Geophysics*, *10*, 453–468. https://doi.org/10.3997/1873-0604.2012027

Kemna, A., Huisman, J., Zimmerman, E., Martin, R., Zhao, Y., Treichel, A., et al. (2014). Broadband electrical impedance tomography for subsurface characterization using improved corrections of electromagnetic coupling and spectral regularization. In Weber, M. & Münch, U. (Eds.), *Tomography of the earth's crust: From geophysical sounding to real-time monitoring. Advanced Technologies in Earth Sciences*. Cham, Switzerland: Springer. https://doi.org/10.1007/978-3-319-04205-3_1

Klinkenberg, L. J. (1941). *The permeability of porous media to liquids and gases*. In *Drilling and production practice* (API-41–200). Washington, DC: American Petroleum Institute.

Koch, K., Kemna, A., Irving, J., & Holliger, K. (2011). Impact of changes in grain size and pore space on the hydraulic conductivity and spectral induced polarization response of sand. *Hydrology and Earth System Sciences*, *15*, 1785–1794. https://doi.org/10.5194/hess-15-1785-2011

Kruschwitz, S., Binley, A., Lesmes, D., & Elshenawy, A. (2010). Textural controls on low-frequency electrical spectra of porous media. *Geophysics*, *75*, WA113–WA123.

Kruschwitz, S., Prinz, C., & Zimathies, A. (2016). Study into the correlation of dominant pore throat size and SIP relaxation frequency. *Journal of Applied Geophysics*, *135*, 375–386. https://doi.org/10.1016/j.jappgeo.2016.07.007

Leroy, P., Li, S., Jougnot, D., Revil, A., & Wu, Y. (2017). Modelling the evolution of complex conductivity during calcite precipitation on glass beads. *Geophysical Journal International*, *209*, 123–140. https://doi.org/10.1093/gji/ggx001

Leroy, P., Revil, A., Kemna, A., Cosenza, P., & Ghorbani, A. (2008). Complex conductivity of water-saturated packs of glass beads. *Journal of Colloid and Interface Science*, *321*, 103–117. https://doi.org/10.1016/j.jcis.2007.12.031

Lesmes, D. P., & Frye, K. K. M. (2001). Influence of pore fluid chemistry on the complex conductivity and induced polarization responses of Berea sandstone. *Journal of Geophysical Research*, *106*, 4079–4090. https://doi.org/10.1029/2000JB900392

Meyerhoff, S. B., Maxwell, R. M., Revil, A., Martin, J. B., Karaoulis, M., & Graham, W. D. (2014). Characterization of groundwater and surface water mixing in a semiconfined karst aquifer using time-lapse electrical resistivity tomography. *Water Resources Research*, *50*, 2566–2585. https://doi.org/10.1002/2013WR013991

Niu, Q., Revil, A., & Saidian, M. (2016). Salinity dependence of the complex surface conductivity of the Portland sandstone. *Geophysics*, *81*, D125–D140. https://doi.org/10.1190/geo2015-0426.1

Nordsiek, S., & Weller, A. (2008). A new approach to fitting induced-polarization spectra. *Geophysics*, *73*, F235. https://doi.org/10.1190/1.2987412

Pape, H., Riepe, L., & Schopper, J. (1987). Theory of self-similar network structures in sedimentary and igneous rocks and their investigation with microscopical and physical method. *Journal of Microscopy*, *148*, 121–147.

Pokrovsky, O. S., Schott, J., & Thomas, F. (1999). Dolomite surface speciation and reactivity in aquatic systems. *Geochimica et Cosmochimica Acta*, *63*, 3133–3143. https://doi.org/10.1016/S0016-7037(99)00240-9

Revil, A. (2012). Spectral induced polarization of shaly sands: Influence of the electrical double layer. *Water Resources Research*, *48*, W02517. https://doi.org/10.1029/2011WR011260

Revil, A. (2013). Effective conductivity and permittivity of unsaturated porous materials in the frequency range 1 mHz-1 GHz. *Water Resources Research*, *49*, 306–327. https://doi.org/10.1029/2012WR012700

Revil, A., Binley, A., Mejus, L., & Kessouri, P. (2015). Predicting permeability from the characteristic relaxation time and intrinsic formation factor of complex conductivity spectra. *Water Resources Research*, *51*, 6672–6700. https://doi.org/10.1002/2015WR017074

Revil, A., & Florsch, N. (2010). Determination of permeability from spectral induced polarization in granular media. *Geophysical Journal International*, *181*, 1480–1498. https://doi.org/10.1111/j.1365-246X.2010.04573.x

Revil, A., Florsch, N., & Camerlynck, C. (2014). Spectral induced polarization porosimetry. *Geophysical Journal International*, *198*, 1016–1033. https://doi.org/10.1093/gji/ggu180

Revil, A., Karaoulis, M., Johnson, T., & Kemna, A. (2012). Review: Some low-frequency electrical methods for subsurface characterization and monitoring in hydrogeology. *Hydrogeology Journal*, *20*, 617–658. https://doi.org/10.1007/s10040-011-0819-x

Revil, A., Koch, K., & Holliger, K. (2012). Is it the grain size or the characteristic pore size that controls the induced polarization relaxation time of clean sands and sandstones? *Water Resources Research*, *48*, W05602. https://doi.org/10.1029/2011WR011561

Revil, A., & Skold, M. (2011). Salinity dependence of spectral induced polarization in sands and sandstones. *Geophysical Journal International*, *187*, 813–824. https://doi.org/10.1111/j.1365-246X.2011.05181.x

Schwarz, G. (1962). A theory of the low-frequency dielectric dispersion of colloidal particles in electrolyte solution. *Journal of Physical Chemistry*, *66*, 2636–2642. https://doi.org/10.1021/j100818a067

Scott, J. B. T., & Barker, R. D. (2003). Determining pore-throat size in Permo-Triassic sandstones from low-frequency electrical spectroscopy. *Geophysical Research Letters*, *30*(9), 1450. https://doi.org/10.1029/2003GL016951

Skold, M., Revil, A., & Vaudelet, P. (2011). The pH dependence of spectral induced polarization of silica sands: Experiment and modeling. *Geophysical Research Letters*, *38*, L12304. https://doi.org/10.1029/2011GL047748

Slater, L. (2007). Near surface electrical characterization of hydraulic conductivity: From petrophysical properties to aquifer geometries—A review. *Surveys in Geophysics*, *28*, 169–197. https://doi.org/10.1007/s10712-007-9022-y

Slater, L., Ntarlagiannis, D., Curatola, F., Pappas, D., Le Roy, D., Evdokimov, K., Rutgers State University of New Jersey, Ontash & Ermac Inc. (2013). *Intelligent spectral induced polarization measurement module*. U.S. Patent US20140218037A1. Washington, DC: U.S. Patent and Trademark Office.

Slater, L. D., & Lesmes, D. (2002). IP interpretation in environmental investigations. *Geophysics*, *67*, 77. https://doi.org/10.1190/1.1451353

Somasundaran, P., & Agar, G. E. (1967). The zero point of charge of calcite. *Journal of Colloid and Interface Science*, *24*, 433–440. https://doi.org/10.1016/0021-9797(67)90241-X

Thompson, D. W., & Pownall, P. G. (1989). Surface electrical properties of calcite. *Journal of Colloid and Interface Science*, *131*, 74–82. https://doi.org/10.1016/0021-9797(89)90147-1

Vinegar, H., & Waxman, M. (1984). Induced polarization of shaly sands. *Geophysics*, *49*, 1267–1287.

Weller, A., Breede, K., Slater, L., & Nordsiek, S. (2011). Effect of changing water salinity on complex conductivity spectra of sandstones. *Geophysics*, *76*, F315–F327.
Weller, A., & Slater, L. (2012). Salinity dependence of complex conductivity of unconsolidated and consolidated materials: Comparisons with electrical double layer models. *Geophysics*, *77*, D185. https://doi.org/10.1190/geo2012-0030.1
Weller, A., Slater, L., Binley, A., Nordsiek, S., & Xu, S. (2015a). Permeability prediction based on induced polarization: Insights from measurements on sandstone and unconsolidated samples spanning a wide permeability range. *Geophysics*, *80*, D161–D173.
Weller, A., Slater, L., Huisman, J. A., Esser, O., & Haegel, F. (2015b). On the specific polarizability of sands and sand-clay mixtures. *Geophysics*, *80*, A57–A61.
Weller, A., Slater, L., & Nordsiek, S. (2013). On the relationship between induced polarization and surface conductivity: Implications for petrophysical interpretation of electrical measurements. *Geophysics*, *78*, D315–D325. https://doi.org/10.1190/geo2013-0076.1
Weller, A., Slater, L., Nordsiek, S., & Ntarlagiannis, D. (2010). On the estimation of specific surface per unit pore volume from induced polarization: A robust empirical relation fits multiple data sets. *Geophysics*, *75*, WA105–WA112. https://doi.org/10.1190/1.3471577
Weller, A., Zhang, Z., Slater, L., Kruschwitz, S., & Halisch, M. (2016). Induced polarization and pore radius—A discussion. *Geophysics*, *81*, D519–D526. https://doi.org/10.1190/geo2016-0135.1
Zhang, Z., & Weller, A. (2014). Fractal dimension of pore-space geometry of an Eocene sandstone formation. *Geophysics*, *79*, D377–D387.